BİTLİS EREN ÜNİVERSİTESİ
FEN BİLİMLERİ DERGİSİ

ISSN: 2147-3129 / e-ISSN: 2147-3188

Article Type	: Research Article	**Year**	: 2025
Received	: February 19, 2025	**Volume**	: 14
Revised	: June 27, 2025	**Issue**	: 3
Accepted	: September 20, 2025	**Pages**	: 1385-1402
DOI	: 10.17798/bitlisfen.1642986		

COMPREHENSIVE ANALYSIS ON THE STRUCTURAL PROPERTIES OF BBIBA:V_2O_5 GLASSES

Melek FİDAN [1]

[1] *Atatürk University, Department of Physics, Erzurum, Türkiye, mbahadir@atauni.edu.tr*

ABSTRACT

This study focuses on the structural characterization of $35B_2O_3$ + (20-x)Bi_2O_3 + xBaO + 19ZnO + $25TeO_2$ + $1V_2O_5$ (x = 0, 5, 10, 15) (BBiBa) glass systems, along with a comprehensive discussion of the obtained findings. The melt quenching process was employed to fabricate the glass samples, and several characterisation methods, including FTIR, Raman spectroscopy, UV-vis spectroscopy, EPR, and XRD, were utilised to assess structural features. FTIR and Raman spectra revealed the existence of bismuth oxide, multiple borate, and telluride groups. Optical absorption spectra exhibited bands at 13736 cm^{-1} and 19881 cm^{-1}, corresponding to the $^2B_{2g} \rightarrow {}^2E_{2g}$ and $^2B_{2g} \rightarrow {}^2B_{1g}$ transitions, respectively. As the BaO content increases, the optical band gaps gradually decrease due to the rise in non-bridging oxygen atoms, which significantly influence the electronic structure. The EPR spectra of VO^{2+} ions exhibited Spin-Hamiltonian parameters satisfying the relation $g_{\parallel} < g_{\perp} < g_e$ and $A_{\parallel} > A_{\perp}$, strongly indicating that the VO^{2+} ions are situated in octahedral sites with a tetragonal distortion. In BaO, the extent of both increase and degradation diminishes. The molecular orbital coefficients further confirm the predominantly covalent character of the ligand bonds.

Keywords: Borotellürite glasses, FTIR, Raman, Optical properties and VO^{2+} ions.

1 INTRODUCTION

Glass exhibits a unique combination of properties, including durability, transparency, ease of fabrication, and cost-effectiveness. Furthermore, its versatile compositional possibilities have elevated its applications beyond mere decorative or household items [1,2]. Glass finds extensive application in diverse fields such as radiation shielding, healthcare, optical fiber communication, solar panels, touchscreens, the automotive industry, architecture, and energy

production. The durability and reliability of glass products are crucial in these applications. Consequently, understanding the mechanical properties of glass, such as elastic modulus and hardness, is essential for enhancing the quality and performance of glass products [1-4]. Ionizing radiation plays a significant role in various aspects of daily life, with applications spanning medicine, agriculture, engineering, industry, and numerous other fields. To safeguard individuals from the adverse effects of radioactive environments, research and development efforts have prioritized the production of highly efficient glasses with superior radiation shielding capabilities [5,6].

Radiation shielding materials are typically alloys composed of various metals combined with their oxide, fluoride, or chloride compounds. Among these, lead is frequently used due to its high density and excellent shielding properties; however, it poses significant risks to both human health and the environment. Glass materials, on the other hand, offer advantages such as high transparency, elevated density, a high effective atomic number, and excellent corrosion resistance. Notably, lead-free glass is non-toxic and demonstrates outstanding resilience to environmental conditions [7-9]. The incorporation of heavy metal oxides (HMOs) into glass enhances its attenuation capability. Research has demonstrated a linear correlation between density and attenuation efficiency, highlighting the significant effectiveness of HMOs in radiation shielding applications [10-12].

Boron oxide (B_2O_3), a key glass network former, is characterized by its low melting point and viscosity, as well as its robust mechanical and thermal properties. It also possesses the ability to interact with a variety of chemicals, facilitating the formation of multicomponent glasses. Within the glass structure, borate exists as two distinct coordination forms—trigonal BO_3 and tetrahedral BO_4—making it an ideal matrix for hosting metal ions [13,14]. However, borate alone is inadequate for shielding applications due to its low atomic number. To enhance its properties, heavy metal oxides (HMOs) and other oxidized compounds have been incorporated into borate-based glasses as modifiers, and their effects have been extensively studied [15-18]. Heavy metal oxides (HMOs) such as Bi_2O_3, ZnO, TeO_2, and BaO enhance the mechanical strength and stability of glass by modifying the glass network through occupation of interstitial sites. The interaction between HMOs and the host matrix results in improvements in transparency, reduced absorption, and potential alterations to the optical band gap of the glass. Borate glasses containing HMOs are widely utilized in technological applications due to their high refractive index and exceptional optical properties [14,19,20]. The addition of barium oxide and bismuth oxide to glass compositions enhances their density, owing to the high

effective atomic number and molecular mass of these heavy metals. This characteristic makes them effective as barriers against harmful radiation [21]. Both barium and bismuth have been shown to possess excellent gamma radiation shielding properties, while also being non-toxic [22]. The substitution of lead with barium and bismuth in glass formulations not only renders the radiation shielding glass non-toxic but also contributes to structural improvements. Tellurium dioxide (TeO_2) is recognized for its high mechanical strength and chemical resistance, along with the unique optical and electrical properties of its tellurite compounds, which are widely utilized in applications such as optical fibers, glass coatings, and electronic devices. Tellurite is characterized by a lower phonon energy, enhancing its ability to conduct and lase effectively [4]. The incorporation of alkaline earth oxides into borotellurite glasses influences their spectroscopic and optical properties, leading to a reduction in the glass transition temperature. The incorporation of transition metal (TM) ions into glass compositions leads to modifications in the magnetic, optical, and electrical properties of the material, with these changes being dependent on the specific composition. Vanadium oxide (V_2O_5) is typically integrated into the structure of oxide glasses as paramagnetic V^{4+} ions, and more frequently as stable oxo-vanadium molecular ions (VO^{2+} or vanadyl), enabling detailed investigation through Electron Paramagnetic Resonance (EPR) spectroscopy [19, 23-25].

This study examines the influence of varying barium and bismuth oxide concentrations on the structural and mechanical properties of borotellurite glass modified with zinc oxide (ZnO) and vanadium oxide (V_2O_5). Beyond their well-established reputation as radiation shielding materials, bismuth and barium also play intriguing roles in altering the magnetic, optical, and electrical properties of materials. Both the total amount of modifier oxides and the network-forming components were found to influence structural characteristics of the glass. Gaining insight into how glass networks form and evolve with rising BaO content is crucial. Consequently, the structural and chemical characteristics of the prepared glass samples were examined using various spectroscopic techniques, including X-ray diffraction (XRD), Fourier transform infrared (FTIR) spectroscopy, Raman spectroscopy, UV-visible absorption, and Electron Paramagnetic Resonance (EPR) spectroscopy.

2 MATERIALS AND METHODS

For the present study, the following compositions were chosen: $35B_2O_3 + (20\text{-}x)Bi_2O_3 + xBaO + 19ZnO + 25TeO_2 + 1V_2O_5$ (x = 0, 5, 10, 15)The starting materials used in the present study were of analar grade: B_2O_3 (99.9%), BaO (99.5%), Bi_2O_3 (99.5%), ZnO (99.9%), TeO_2

(99%), and V_2O_5 (99.5%). Each chemical batch was weighed up to 8 grams and carefully mixed and ground to obtain a homogeneous mixture. The batches were placed in a porcelain crucible and subsequently melted in an electric furnace at 950°C in air. The molten mixture was poured into a preheated (200°C) granite mold and rapidly cooled. To reduce stress and enhance mechanical strength, the quenched samples were annealed.

An Empyrean XRD single crystal diffractometer manufactured by PANalytical was used to examine the materials' amorphous structure. X-ray diffraction (XRD) analyses were carried out using Cu-Kα radiation (λ = 1.5406 Å) at an operating voltage of 45 kV and a current of 40 mA. Data were recorded over a 2θ range of 10° to 90°, with a step size of 0.026° and a scan rate of 0.05°/s. FTIR and Raman spectra were collected to analyze and characterize the functional groups in the structures. FTIR spectra were obtained using a Bruker VERTEX 70v instrument in the wavenumber range of 50 to 4000 cm^{-1}, while Raman spectra were recorded in the range of 350–1050 nm with a WITec alpha 300R instrument. Both techniques were employed for the same purpose of functional group analysis. A Shimadzu UV-3600 Plus spectrophotometer was used to acquire UV-Vis optical absorption spectra at room temperature, covering the wavelength range of 185 to 3300 nm. Using a Varian E-104 X-band EPR spectrometer at a microwave power of 13 dB, the magnetic field was measured in the range of 2500 to 4500 G, with 2,2-diphenyl-1-picrylhydrazyl (DPPH) serving as the primary field marker.

3 RESULTS AND DISCUSSION

3.1 XRD (X-Ray Diffraction)

The glasses in the amorphous structure exhibit some order at short distances, although they lack the clear pattern characteristic of crystals at longer distances. X-ray diffraction is effective for elucidating the non-crystalline framework of a glass system. Figure 1 displays the XRD image pattern of BBiBa glasses, where a prominent peak observed within the 2θ range of 28–30° indicates their amorphous character [26-28]. As the BaO content increases in the studied samples—particularly at 15 mol%—noticeable variations are observed in the XRD peaks. While amorphous glass-like structures lack long-range order, changes in interplanar spacing caused by factors such as thermal expansion, internal stress, or the incorporation of impurities can still influence the angular position of the XRD peak.

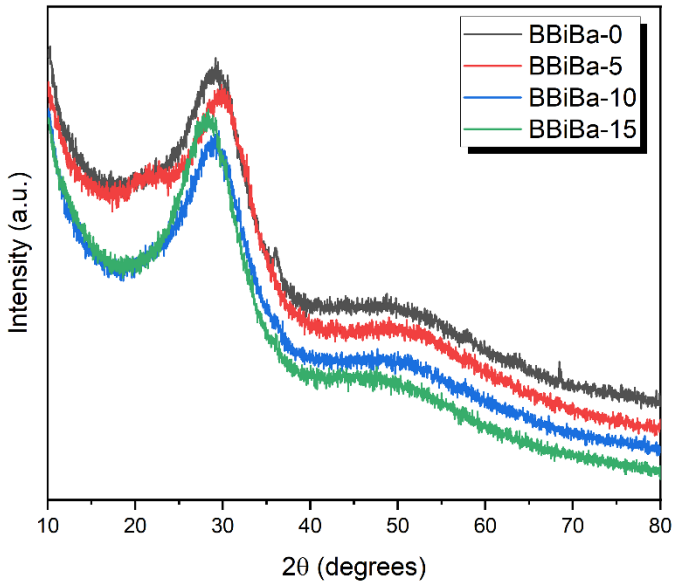


Figure 1. XRD patterns for the BBiBa glass

3.2 FTIR (Fourier Transformation Infrared Spectroscopy)

Infrared spectroscopy offers quantitative insights into the structure of glass samples and serves as an excellent approach for investigating structural disorder in glasses. The FTIR spectra of the glass sample analysed in this investigation are presented in the figure 2 and the observed bands are listed in Table 1.

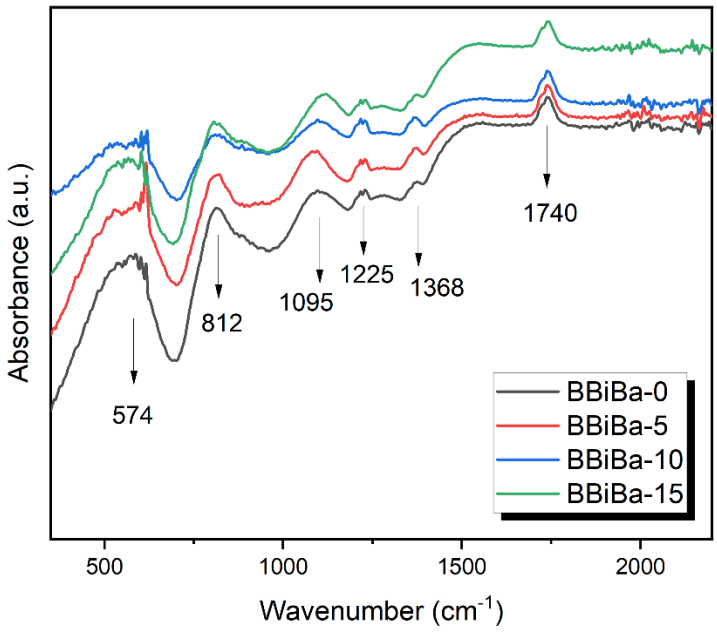


Figure 2. FTIR spectra of BBiBa glasses

Table 1. Assignments of IR bands of BBiBa glass system

IR bands (cm^{-1})	Assignment
574	The stretching vibrations of Bi-O bonds within BiO_6 units
812	Symmetric stretching vibrations of B–O bonds in BO_4 group
1095	Stretching vibrations of B-O bonds in BO_4 units from tri-, tetra-, and penta-borate groups
1225	Symmetric stretching vibration of BO_3 groups
1368	Non-symmetric stretching vibrations of B–O of trigonal BO_3 units
1740	stretching vibration of nonbridging oxygen atoms (NBOs) in BO_3 species

The FTIR spectra in the present investigation exhibit several bands at 574, 812, 1095, 1225, 1368, and 1740 cm^{-1}, as illustrated in Figure 2. The band at around 574 cm^{-1} arises from the stretching vibrations of Bi-O bonds within BiO_6 units exhibiting a deformed octahedral structure [20,25,29,30]. The IR characteristics situated in the first area that ranges between 1200 and 1600 cm^{-1} are attributable to the asymmetric stretching vibration of B–O bonds from the BO_3 trigonal units. The second region's spectrum characteristics, which cover 800–1200 cm^{-1}, are caused by the BO_4 tetrahedral units' B–O bond stretching. The third region 400 - 800 cm^{-1} can be attributed to the different B-O-B bending modes in BO_3 and BO_4 [14,23,31]. The B–O symmetric stretching vibration in the BO_4 units of the glass matrix is observable in the spectral band at 812 cm^{-1} [32,33]. The broad band at 1095 cm^{-1} is attributed to the B–O stretching vibrations in the BO_4 units of triborate, tetraborate, and pentaborate groups [20, 34,35]. The small peak at 1225 cm^{-1} in BBiBa glasses has been assigned to B-O stretching vibrations of $(BO_3)_3$ units in metaborate and orthoborate chains [27,36,37]. Asymmetric stretching mode of the B-O moieties of the trigonal units BO_3 is represented by a tiny peak at 1368 cm^{-1} [38,39]. The final band of the spectra, which was detected at 1740 cm^{-1}, has been ascribed to the B-O stretching modes of the NBO of BO_3 units [3,37,40].

3.3 Raman Spectroscopy

Raman spectroscopy offers structural insights, including significant chemical bonds, molecular vibrations, and atomic interactions within the glass sample. The Raman spectra of all the glasses are represented in Figure 3.

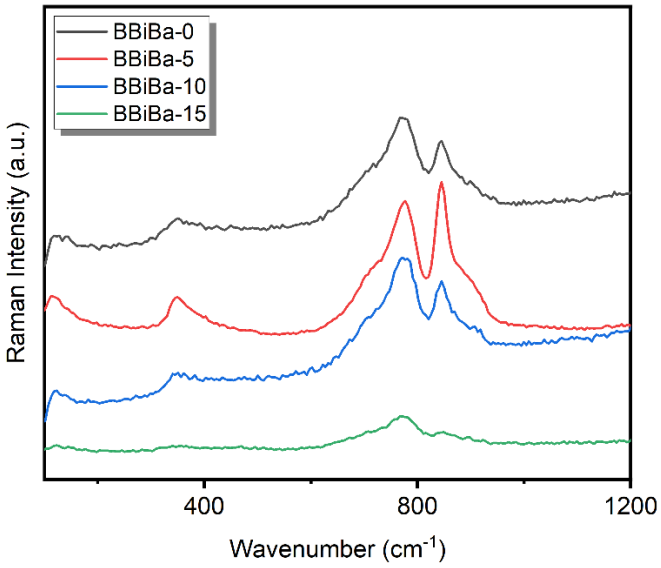


Figure 3. Raman spectra of BBiBa glasses

Raman spectra exhibit four distinct areas for glasses incorporating heavy metal oxides (Bi_2O_3, BaO, PbO, etc.): 1) Low wavenumber acoustic Raman modes (<100 cm^{-1}), 2) Heavy metal (HM) ion vibrations in the 70-160 cm^{-1} region, 3) Bridged anion (BA) vibrations in the range of 300-600 cm^{-1}, 4) Vibrations of non-bridged anions (NBA) at higher wavenumbers [21,41,42]. The peaks observed and the assignments to which they belong are listed in Table 2.

Table 2. BBiBa glass system Raman band allocation

IR bands (cm^{-1})	Assignment
120	vibrations of heavy metal ions Bi^{3+}
347	stretching vibrations of Bi-O-Bi
702	Te–O stretching vibrations in TeO_4
776	B-O stretching vibrations in the [BO_4] tetrahedral unit, Te-O asymmetric stretching vibrations in the TeO_3 (tp) units
845	Symmetric stretching vibrations of the B-O-B bridge
904	B-O bonding vibrations in BO_3 units

The peaks observed around 120 cm^{-1} in Figure 3 are attributed to Bi^{3+} cations from [BiO_3] and [BiO_6] groups. The fact that the band is located at low wave numbers confirms the presence of octahedral units [BiO_6] in the glass structure [37,43,44]. The peaks between 120-600 cm^{-1} correspond to bridging anion vibrations, while the band at 347 cm^{-1} is ascribed to Bi-O-Bi stretching vibrations [20,45,46]. The symmetrical stretching vibrations of Te-O in TeO_4 units are responsible for the small, broad shoulder at around 702 cm^{-1} [36,43,47]. The sharp peak at 776 cm^{-1} in the Raman spectra corresponds to the B-O symmetric stretching vibrations

of the BO_3/BO_4 structural units [41,48]. Furthermore, this Raman peak can potentially be attributed to the Te-O asymmetric stretching vibrations in the TeO_3 (tp) units [36,49,50]. The Raman band at 845 cm^{-1} is due to the symmetric stretching vibration of the B-O-B bridge of the pyroborate units [41,51]. The weak peak at 904 cm^{-1} indicates the presence of B-O bond vibrations in the [BO_3] ortho-borate groups of the triangular units [37,44]. As BaO substitution increases, the intensity of these Raman bands diminishes and, with except for the peaks at 776 and 845 cm^{-1}, others almost completely disappear, as shown in Figure 3. With the incorporation of BaO, significant variations in the intensities of the Raman peaks and slight shifts in their positions were observed. These findings indicate structural modifications within the glass network.

3.4 UV-Vis (Ultraviolet-Visible Spectroscopy)

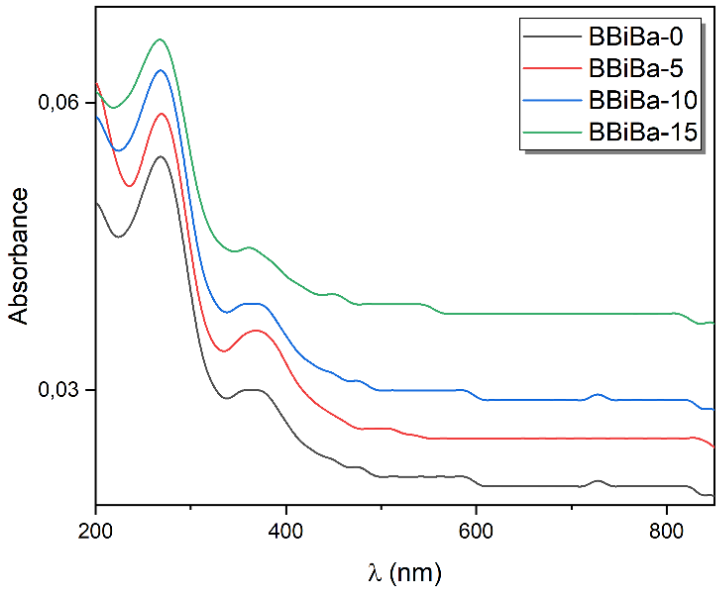


Figure 4. Optical absorption spectra of BTLC glasses

The UV–Vis absorption spectra of VO^{2+} doped BBiBa glass samples were acquired at room temperature within the spectral range of 200-850 nm and is shown in Figure 4. The vanadyl ion possesses the electronic configuration of [Ar] $3d^1$ in the +4-oxidation state and exhibits paramagnetic characteristics in VO^{2+} complex ions, with the ground state of VO^{2+} being ^2D. The degenerate $^2T_{2g}$ and ^2E_g energy levels are separated into $^2B_{2g}$, ^2E_g, and $^2B_{1g}$, $^2A_{1g}$ sublevels, respectively, in the tetragonally compressed octahedral environment. The optical absorption bands for the studied glasses are assigned to the $^2B_{2g} \rightarrow {}^2A_{1g}$, $^2B_{2g} \rightarrow {}^2B_{1g}$ and

$^2B_{2g} \rightarrow {}^2E_g$ electronic transitions. The $^2B_{2g} \rightarrow {}^2A_{1g}$ transition is responsible for a faint band near 480 nm and the $^2B_{2g} \rightarrow {}^2B_{1g}$ transition for a band that appears only prominently at 370 nm at the absorption edge of the glass host in the optical absorption spectra [24,36,52-54]. The optical absorption spectra indicate that the fundamental absorption edge is not distinctly defined, emphasising the glassy characteristics of the materials. Table 3 indicates the cut-off wavelengths ($\boldsymbol{\lambda_c}$) of the present glass samples with another parameter. As the BaO content of the samples increases, the cut-off wavelength shifts towards longer wavelengths.

Table 3. Summary of optical absorption data for BBiBa glasses.

Sample	$\boldsymbol{\lambda_c(nm)}$	$\boldsymbol{E_{ind}(eV)}$	$\boldsymbol{E_d(eV)}$	$\boldsymbol{E_u(eV)}$
BBiBa-0	336	3.446	3.725	0.340
BBiBa-5	342	3.352	3.683	0.370
BBiBa-10	349	3.280	3.642	0.424
BBiBa-15	364	3.124	3.580	0.538

Tauc's theory estimates the band gap energy, both direct and indirect, of glasses using the Davis and Mott relations [55,56].

$$\alpha(v)hv = A\left(hv - E_g\right)^n \tag{1}$$

The energy of the optical band gap (E_g), the constant A, and the exponent n are crucial parameters for determining the kind of transition; n values of 2 and 1/2 signify allowed direct and indirect transitions for the oxide glasses, respectively. By projecting the linear segment of the indirect and direct transition curve to $\alpha = 0$, the optical band gap (E_g) values can be determined (refer to Figure 5 and 6). The data for both direct and indirect transitions, presented in Table 3, indicate that the band gap diminishes with increasing BaO content. In the glass matrix, non-bridging oxygens (NBOs) exhibit a weaker bond to electrons compared to bridging oxygens (BOs), indicating that less energy is necessary to promote an electron to the conduction band. In existing glasses, it may be stated that BOs convert into NBOs as E_g values reduce. The noted consequence is completely consistent with studies that have been reported in the literature [24,30,57,58].

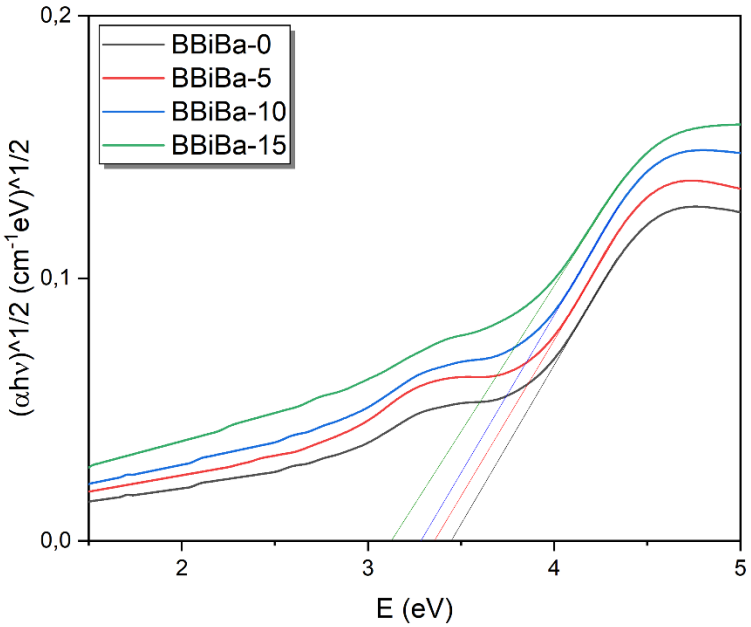


Figure 5. $(\alpha h\nu)^{1/2}$ vs E=hν of the BTLC glasses

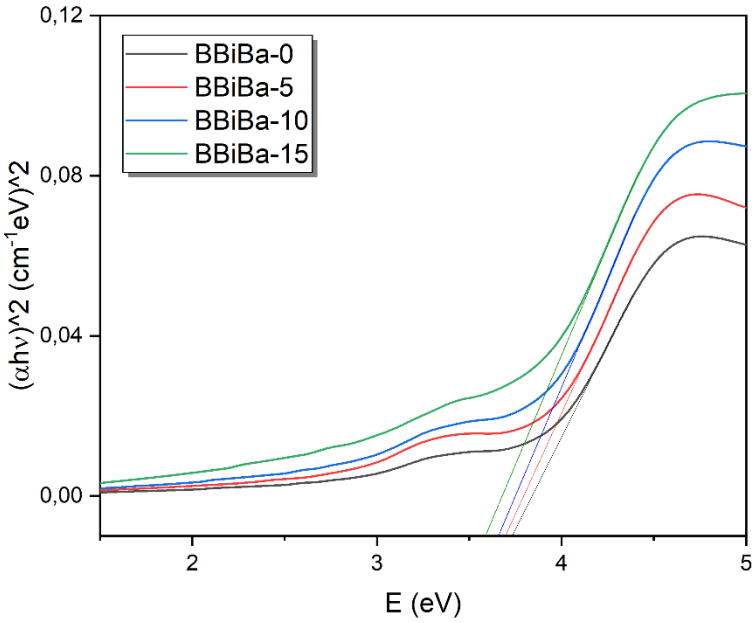


Figure 6. $(\alpha h\nu)^2$ vs E=hν of the BTLC glasses

In the final analysis, an increase in the Urbach energy, another quantity in Table 3, results from an increase in the BaO content. Figure 7 shows the Urbach curve for BBiBa glasses. The presence of BaO in the glass as a modifier and an increase in the concentration of NBO are indicated by the rise in the Urbach energy, which is used to quantify structural disorder [4,37,59,60].

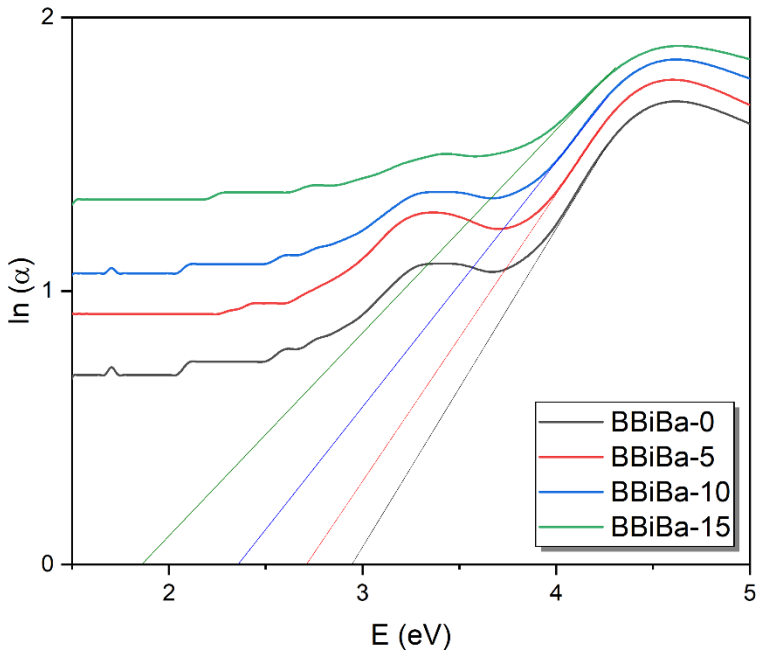


Figure 7. Urbach plots for BTLC glasses

3.5 EPR (Electron Paramagnetic Resonance) Measurements

The electron paramagnetic resonance technique is highly effective for elucidating the local environment surrounding transition metal (TM) ions. TM ions integrated into the glass matrix alter the glass structure by interacting with the surrounding ligands through ligand domains [52,61]. As seen in Figure 8, the EPR spectra of glasses features a hyperfine structure comprising sixteen lines (eight perpendicular and eight parallel) indicative of the unpaired electron ($3d^1$) of the VO^{2+} ion associated with ^{51}V (I = 7/2) exhibiting axial symmetry. Comparable EPR signals have been documented in several glass matrices infused with V_2O_5 [24,58,62-65]. The EPR spectra were examined in accordance with the Hamiltonian for axial symmetry as follows [66].

$$\mathcal{H} = \beta g_{\parallel} B_z S_z + \beta g_{\perp}\left(B_x S_x + B_y S_y\right) + A_{\parallel} S_z I_z + A_{\perp}\left(S_x I_x + S_y I_y\right) \quad (2)$$

In this context, the terminology follows the definitions provided in the relevant reference [4]. The spin–orbit interaction was included in the g values, and nuclear Zeeman and quadrupole interactions were disregarded due to their negligible effects.

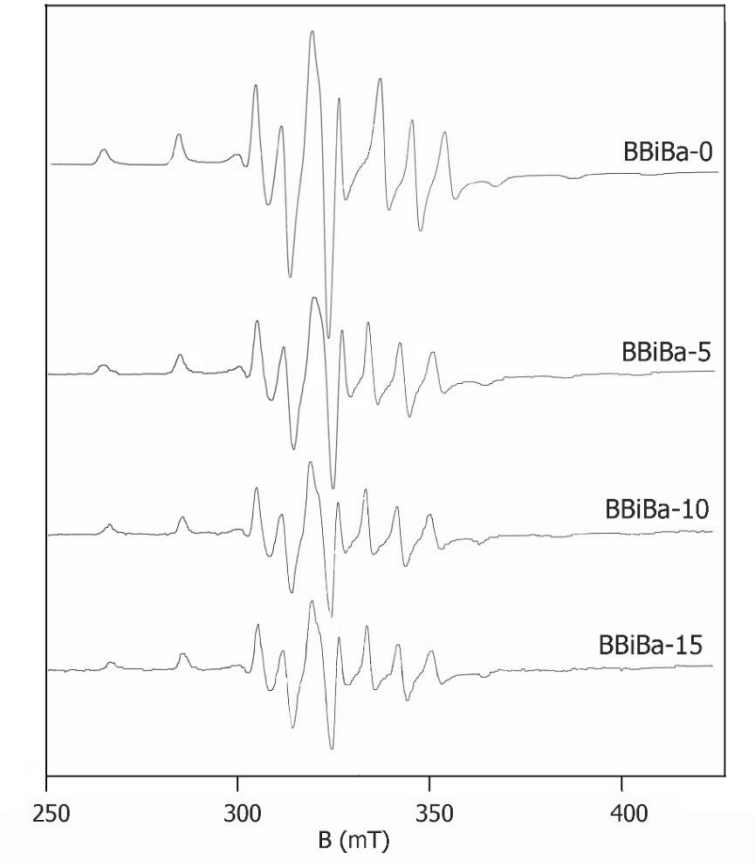


Figure 8. EPR spectra of BBiBa:VO^{2+} glasses

A definition of the spin-Hamiltonian solutions for parallel and perpendicular hyperfine lines is provided below:

$$B_{\parallel}(m_I) = B_{\parallel}(0) - A_{\parallel}m_I - A_{\perp}^2\,[I(I+1) - m_I^2]/2B_{\parallel}(0) \tag{3a}$$

$$B_{\perp}(m_I) = B_{\perp}(0) - A_{\perp}m_I - \left(A_{\perp}^2 + A_{\parallel}^2\right)[I(I+1) - m_I^2]/4B_{\perp}(0) \tag{3b}$$

where $B_{\parallel}(0)$ and $B_{\perp}(0)$ are the centre values from the first derivative curve that correspond to $g_{\parallel}$ and $g_{\perp}$ components, respectively, and m_I is the magnetic quantum number of the vanadium nucleus. The spin-Hamiltonian parameters (SHP) $g_{\parallel}$, $g_{\perp}$, $A_{\parallel}$, and $A_{\perp}$ were obtained from the equation solutions and are presented in Table 4. The vanadium ion is in the octahedral state under tetragonal compression in the current glasses, with a ground state of C_{4v} symmetry, as can be seen from the SHP value data. The degree of tetragonal distortion is indicated by the $\Delta g_{\parallel}/\Delta g_{\perp}$ value. As observed in the table, the values exhibit an almost linear decrease with increasing BaO content, suggesting that tetragonal compression intensifies as the BaO concentration rises [67-69].

Table 4. Spin-Hamiltonian parameters and molecular orbital coefficients calculated for paramagnetic vanadyl complexes in the BBiBa glasses

Sample code	$g_{\parallel}$	$g_{\perp}$	$A_{\parallel}$	$A_{\perp}$	β^2	$1-\alpha^2$	$1-\gamma^2$	P	κ	$\Delta g_{\parallel}/\Delta g_{\perp}$
BBiBa-0	1.945	1.999	193.6	71.4	0.936	0.234	0.987	133	0.808	17.36
BBiBa-5	1.941	1.999	195	70.7	0.932	0.181	0.857	135	0.798	9.73
BBiBa-10	1.938	1.996	196.4	72.14	0.930	0.139	0.726	135	0.811	7.75
BBiBa-15	1.936	1.990	197.14	72.86	0.930	0.113	0.465	135	0.821	5.39

Optical absorption data (d-d transitions) and EPR investigations (g-values) enabled the calculation of molecular orbital (MO) coefficients. The molecular orbital coefficients of the vanadyl ion were derived by linking optical absorption and EPR data through the following equations [69,70]:

$$A_{\parallel} = P\left[\kappa + \frac{4}{7}\beta^2 + \Delta g_{\parallel} + \frac{3}{7}\Delta g_{\perp}\right] \quad and \quad A_{\perp} = -P\left[\kappa - \frac{2}{7}\beta^2 + \frac{11}{14}\Delta g_{\perp}\right] \tag{4}$$

$$g_{\parallel} = g_e\left(1 - \frac{4\lambda\alpha^2\beta^2}{\Delta_{\parallel}}\right) \qquad and \qquad g_{\perp} = g_e\left(1 - \frac{\lambda\gamma^2\beta^2}{\Delta_{\perp}}\right) \tag{5}$$

where λ =170 cm is the spin–orbit coupling constant of VO^{2+} ion and g_e (2.0023) is the free electron g value. Furthermore, P is dipolar hyperfine coupling parameter and κ is Fermi contact term that quantifies the density of unpaired electrons at the vanadium nucleus. High values of κ suggest that the unpaired s electron substantially influences the hyperfine constant [71]. $1-\gamma^2$ and $1-\alpha^2$ are measure of covalency measures of out-of-plane π- and in-plane σ- bonding with the equatorial ligands, respectively and β^2 describes out-of-plane π-bonding along the $V=O$ bond direction. $\Delta_{\parallel}$ (19881cm^{-1}) and $\Delta_{\perp}$(13736 cm^{-1}) represent the electronic energies corresponding to the $^2B_{2g}\rightarrow{}^2B_{1g}$ and $^2B_{2g}\rightarrow{}^2E_{2g}$ transitions in the absorption spectra of these BBiBa glasses, respectively. The ESR parameters and molecular orbital characteristics, computed using the various aforementioned expressions, are presented in Table 4. Based on the β^2 values in Table 4, the covalence of out-of-plane π bonds in the $V=O$ bond direction remains largely unchanged with the increasing BaO content. However, the π bonds between the equatorial ligands and vanadium atoms exhibit partial covalence and are influenced by the increasing BaO content, leading to a substantial reduction in their covalent character.

4 CONCLUSION

The present work examines the influence of BaO content, introduced as a network modifier, on the structural and physical characteristics of BBiBa:V_2O_5 glasses. Understanding

the structural evolution of the glass network with increasing BaO levels provides valuable information for various applications such as healthcare, optical fiber communications, solar panels, touch screens, automotive industry, architecture and energy production. XRD was primarily employed to investigate the structural properties of BBiBa:V_2O_5 glass, whereas complementary techniques such as FTIR, Raman, UV-Vis spectroscopy, and EPR were utilized to elucidate the chemical framework and bonding environment within the glass matrix, leading to the following conclusions:

In the XRD spectra, the absence of peaks signifying crystalline phases verified the BBiBa glasses' amorphous origin. The findings from FTIR and Raman spectra validate the existence of bismuth oxide inside the structural frameworks of the glass samples, and indicate that it comprises structural units including TeO_4, TeO_3, BO_3, and BO_4. The reduction in direct and indirect band gaps with increasing BaO content corroborates the enhancement of non-bridging oxygen formation. The Urbach energy serves as a key parameter for assessing the structural instability of amorphous materials, where lower values correspond to a reduced degree of glassiness. The Urbach energy indicates a progressive increase in the BaO content within the studied glass system, which has high tendency to convert weak bonds into defects in the BBiBa-15 sample. The optical absorption spectra of the glass samples reveal two absorption bands, characteristic of VO^{2+} ions positioned in octahedral sites with tetragonal distortion. The invariance of the Spin-Hamiltonian parameters g and A with varying BaO content suggests minimal impact on the local electronic environment. However, the substantial reduction in $\Delta \boldsymbol{g}_{\parallel}/\Delta \boldsymbol{g}_{\perp}$ indicates a pronounced distortion of the octahedral coordination around VO^{2+} ions. The $1-\gamma^2$ values suggest strong covalence in out-of-plane π bonds, while the $1-\alpha^2$ values indicate weak covalence in in-plane σ bonds. Additionally, β^2 values confirm strong covalence in out-of-plane $V=O$ bonds, highlighting the anisotropic bonding characteristics within the system.

Statement of Research and Publication Ethics

The study is complied with research and publication ethics.

Artificial Intelligence (AI) Contribution Statement

This manuscript was entirely written, edited, analyzed, and prepared without the assistance of any artificial intelligence (AI) tools. All content, including text, data analysis, and figures, was solely generated by the authors.

REFERENCES

[1] C.Bootjomchai, J.Laopaiboon, C.Yenchai, R.Laopaiboon, Gamma-rayshielding and structural properties of barium–bismuth–borosilicate glasses, *Radiat.Phys. Chem.*, vol. 81, pp. 785– 790, July 2012.

[2] J. S. Alzahrani, A. Hammoud, I. Boukhris, Z.A. Alrowaili, A. V. Lebedev, I.O. Olarinoye, M.S. Al-Buriahi, Fabrication and characterization of TeO_2–Na_2O–BaO glass doped with Yb_2O_3 for optical and particulate-radiation shielding applications: Role of Bi_2O_3/WO_3, *Opt. Mater.*, vol. 150, pp. 115141, April 2024.

[3] A. M. Babeer, H. Y. Amin, M.I. Sayyed, Abd El-razek Mahmoud, M.A. Abdo, T. E. Ellakwa, M.S. Sadeq, Impact of mixed heavy metal cations (Ba and Bi) on the structure, optical and ionizing radiation shielding parameters of Bi_2O_3–BaO–Fe_2O_3–SrO–B_2O_3 glass matrix, *Ceram. Int.*, vol. 50, pp. 19245-19258, June 2024.

[4] M. Fidan, A. Acikgoz, G. Demircan, D. Yilmaz, B. Aktas, Optical, structural, physical, and nuclear shielding properties, and albedo parameters of TeO_2–BaO–B_2O_3–PbO–V_2O_5 glasses, *J. Phys. Chem. Solids*, vol. 163, pp. 110543, April 2022.

[5] Y.S. Alajerami, D. Drabold, M.H.A. Mhareb, Katherine Leslee A. Cimatu, Gang Chen, M. Kurudirek, Radiation shielding properties of bismuth borate glasses doped with different concentrations of Cadmium oxides, *Ceram. Int.*, vol. 46, pp. 12718-12726, June 2020.

[6] H. Abdurabu Thabit, A. Khamim Ismail, H. Es-soufi, D.A. Abdulmalik, A. M. Al-Fakih, S. Alraddadi, M.I. Sayyed, Structural, thermal, and mechanical investigation of telluro-borate-Bismuth glass for radiation shielding, *J. Mater. Res. Technol*, vol. 24, pp. 4353-4363, May-June 2023.

[7] D.A. Aloraini, A.H. Almuqrin, M.I. Sayyed, A. Kumar, Exploring the mechanical behavior and gamma ray attenuation properties of Bi_2O_3–BaO–V_2O_5 glasses, *J Mater Sci: Mater Electron*, vol. 34, pp.1746, September 2023.

[8] A.K. Reza Bagheri, Moghaddam, H. Yousefnia, Gamma ray shielding study of barium-bismuth-borosilicate glasses as transparent shielding materials using MCNP-4 C code, XCOM program, and available experimental data, *Nuclear Eng. Technol.*, vol. 49, pp. 216–223, February 2017.

[9] M.I. Sayyed, M.H.A. Mhareb, I. Alrammah, Ali A.A. Alghamdi, A. Abdullah Alsurayj, S. Talib Alminhali, M. Essam Abdelgawad, Z. Ali Abugurain, N. Alonizan, M. Alqahtani, Gamma ray shielding and structural properties for TeO_2-BaO-MO modified with Bi_2O_3, TiO_2, MnO_2, MoO_3, *Radiat. Phys. Chem*., vol. 205, pp. 110714, April 2023.

[10] H. Aboud, Mohammed J.R. Aldhuhaibat, Y. Alajermi, Gamma radiation shielding traits of B_2O_3–Bi_2O_3–CdO–BaO–PbO glasses, *Radiat. Phys. Chem*, vol. 191, pp. 109836, February 2022.

[11] N. Effendy, M.H.M. Zaid, K.A. Matori, S.M. Iskandar, R. Hisam, M.N. Azlan, N.N. Yusof, Hesham M.H. Zakaly, Shams A.M. Issa, Y.B. Saddeek, Fabrication of novel BaO–Al_2O_3–Bi_2O_3–B_2O_3 glass system: Comprehensive study on elastic, mechanical and shielding properties, *Prog. Nucl. Energy*, vol. 153, pp. 104418, November 2022.

[12] M.I. Sayyed, M.H.A. Mhareb, B. Ceviz Şakar, K.A. Mahmoud, E. Şakar, H. Abdurabu Thabit, Kawa M. Kaky, S.O. Baki, Experimental investigation of structural and radiation shielding features of Li_2O-BaO-ZnO-B_2O_3-Bi_2O_3 glass systems, *Radiat. Phys. Chem*, vol. 218, pp. 111640, May 2024.

[13] A. Kumar, M.I. Sayyed, Taha. A. Hanafy, Physical, mechanical, structural, optical and gamma ray shielding behavior of (90-x-y)B_2O_3–5PbO–5BaO-xZnO-yTiO_2 glasses, *Ceram. Int*., vol. 50, pp. 43279-43288, November 2024..

[14] M.A. Ouis, M.A. Marzouk, Comparative optical, FTIR and photoluminescence spectral analysis of copper ions in BaO–B2O3, SrO– B_2O_3 or Bi2O3– B_2O_3 glasses and impact of gamma irradiation, *J. Lumin*, vol. 223, pp. 117242, July 2020.

[15] S. Biradar, M.N. Chandrashekara, A. Dinkar, Manjunatha, G.B. Devidas, A.S. Bennal, M.I. Sayyed, H. Es-soufi, A multifaceted study of B_2O_3-BaO-PbO-WO_3 glasses doped with Bi2O3: Insights from physical, thermal, structural, mechanical and optical analyses towards improved shielding properties, *Ceram. Int*., vol. 50, pp. 29332-29345, September 2024.

[16] H.O. Tekin, G. Susoy, S. A.M. Issa, A. Ene, Ghada ALMisned, Y.S. Rammah, Fatema T. Ali, M. Algethami, Hesham M.H. Zakaly, Heavy metal oxide (HMO) glasses as an effective member of glass

shield family: A comprehensive characterization on gamma ray shielding properties of various structures, *J. Mater. Res. Technol*, vol. 18, pp. 231-244, May-June 2022.

[17] S. Prakash Singh, R.P.S. Chakradhar, J.L. Rao, B. Karmakar, EPR, FTIR, optical absorption and photoluminescence studies of Fe_2O_3 and CeO_2 doped $ZnO–Bi_2O_3–B_2O_3$ glasses, *J. Alloys Compd*., vol. 493, pp. 256-262, March 2010.

[18] S. Kaewjaeng, S. Kothan, N. Wantana, H.J. Kim, R. Rajaramakrishna, C. Jumpee, P. Limsuwan, J. Kaewkhao, Fabrication luminescence and radiation shielding properties of $Gd_2O_3–La_2O3–ZnO–B_2O_3–Sm_2O_3$ glasses, *Radiat. Phys. Chem*, vol. 202, pp. 110537, January 2023.

[19] L. Srinivasa Rao, AC conductivity and polarization phenomenon of $Li_2O–MoO_3–B_2O_3:V_2O_5$ glasses, *J. Alloys Compd*., vol. 787, pp. 1280-1289, May 2019.

[20] J. Liu, X. Xu, T. Zheng, Y. Guo, J. Lv, Effect of Bi_2O_3 content on the structure and properties of Bi_2O_3-B_2O_3-BaO-ZnO glass, *J. Non-Cryst. Solids*, vol. 575, pp. 121211, January 2022.

[21] [21] P. Kaur, K.J. Singh, S. Thakur, P. Singh, B.S. Bajwa, Investigation of bismuth borate glass system modified with barium for structural and gamma-ray shielding properties, *Spectrochim. Acta - A: Mol. Biomol*., vol. 206, pp. 367-377, January 2019.

[22] E. Kavaz, N. Yıldız Yorgun, Gamma ray buildup factors of lithium borate glasses doped with minerals, *J. Alloys Compd*., vol. 752, pp. 61-67, July 2018.

[23] M. Fidan, A.Acikgoz, D. Yılmaz, G. Demircan, S. Kalecik, B. Aktas, S. Isgor, Investigation of the structural, mechanical, radiation and neutron shielding properties of the TeO_2-B_2O_3-Li_2O-MoO_3-CuO glass system*, J. Alloys Compd*., vol. 976, pp. 172981, March 2024.

[24] B.V. Padlyak, T.B. Padlyak, Spectroscopic properties of the V-doped borate glasses, *J. Non-Cryst. Solids*, vol. 528, pp. 119741, January 2020.

[25] T. Annapurna, M. Kostrzewa, A. Siva Sesha Reddy, A. Ingram, J. Ashok, V. Ravi Kumar, N. Veeraiah, Polaronic conduction and dielectric relaxation dynamics in V_2O_5 added lead bismuth silicate glass system, *J. Non-Cryst. Solids*, vol. 528, pp. 119746, January 2020.

[26] V. Sreenivasulu, G. Upender, V. Chandra Mouli, M. Prasad, Structural, thermal and optical properties of $TeO_2–ZnO–CdO–BaO$ glasses doped with VO^{2+}, *Spectrochim. Acta - A: Mol. Biomol*., vol. 148, pp. 215-222, September 2015.

[27] J. Zheng, H. Wang, S. Lin, Z. Pan, Q. Yang, J. Liu, Spectral characteristics of highly thermally stable Eu^{3+}-doped P_2O_5-B_2O_3-ZnO-BaO glasses for tricolor WLEDs and red lasers, *J. Alloys Compd*., vol. 1010, pp. 177668, January 2025.

[28] Ö. F.Ötken, İ. Ceylan, B. Çiçek, High-temperature aqueous corrosion of $MO–Na_2O–B_2O_3–SiO_2$ glass and glass-ceramic coatings on metallic substrates: Effect of alkaline earth metals M^{2+}= {Ca^{2+}, Sr^{2+}, Ba^{2+}}, J. *Eur. Ceram. Soc.,* vol. 45, pp. 116820, Jaunary 2025.

[29] L. Zhang, Q. Sun, J. Wang, Z. Zhang, W. Zhang, J. Wang, H. Chen, M. Li, Effect of SrO content on microstructure of Bi_2O_3-B_2O_3-ZnO-BaO-SrO low-melting glass frit and joining performance of sodalime glass substrates, *J. Alloys Compd*., vol. 872, pp. 159707, August 2021.

[30] M.I. Sayyed, H.O. Tekin, Malaa M. Taki, M.H.A. Mhareb, O. Agar, E. Şakar, Kawa M. Kaky, Bi_2O_3-B_2O_3-ZnO-BaO-Li_2O glass system for gamma ray shielding applications, *Optik*, vol. 201, pp. 163525, January 2020.

[31] M.S. Sadeq, A.S. Sharafelden, Fifi M. Reda, Mona H. Ibrahim, Effect of ZnO on the structure, optical properties and ESR studies of $B_2O_3–Na_2O–SrO–Fe_2O_3–ZnO$ glass system, *Ceram. Int*., vol. 51, pp. 4878-4890, February 2025.

[32] Kh. S. Shaaban, D. A. Aloraini, K. Alsafi, H. M. Almutairi, W. M. Al-Saleh, A.S. Alzahrani, Role of CeO_2 in the enhancement of the properties of the SiO_2-B_2O_3-BaO-Li_2O-glass system: Structural, mechanical and radiation shielding study, *Mater. Today Commun*., vol 38, pp. 108309, March 2024.

[33] A. E. Mwakuna, C. Laxmikanth, R.K.N.R. Manepalli, Effect of replacing B_2O_3 with CuO on the structural, optical absorption, thermal, mechanical, and gamma-ray shielding properties of $B_2O_3–Bi_2O_3–K_2O$ glass, *Opt. Mater*., vol. 157, pp. 116282, November 2024.

[34] E. Mansour, FTIR spectra of pseudo-binary sodium borate glasses containing TeO_2, *J. Mol. Struct*., vol. 1014, pp. 1-6, April 2012.

[35] R. E. M. Khaidir, Y. W. Fen, M. H. Mohd Zaid, K. A. Matori, N. A. Sheh Omar, M. Fahmi Anuar, S.A. Abdul Wahab, A. Z. Khirel Azman, Optical band gap and photoluminescence studies of Eu^{3+}-doped zinc silicate derived from waste rice husks, *Optik*, vol. 182, pp. 486-495, April 2019.

[36] M. Anand Pandarinath, P. Muralikrishna, D. Suresh Babu, B. Vijaya Kumar, G. Upender, Vibrational, thermal and optical studies of $30TeO_2$-$39.5B_2O_3$-(30-x)ZnO-xLi_2O-$0.5V_2O_5$ ($0 \leq x \leq 30$ mol%) glass system, *J. Non-Cryst. Solids*, vol. 566, pp. 120875, August 2021.

[37] I. Saber, K. Dahmani, M. Galai, A. EL Magri, R. Hsissou, H. Barbita, M. Belfaquir, I. Warad, N. AL-Zaqri, M.S. Elyoubi, Synthesis and characterization of new eco-friendly vitreous system Bi_2O_3–B_2O3–BaO: Structural, morphologic, and thermal analysis, *Opt. Mater.*, vol. 149, pp. 115079, March 2024.

[38] S.N. Nazrin, A. Amat, Shams A.M. Issa, Hesham M.H. Zakaly, S. S. Gunasekaran, H. B. Zaman, M.H.M. Zaid, M.H.M. Tahir, Ibrahim A. Shaaban, I. Sharma, Elastic and radiation shielding properties of zinc borotellurite glass systems: The impact of gadolinium oxide, *Opt. Mater.*, vol. 157, pp. 116252, November 2024.

[39] T. Satyanarayana, I. V. Kityk, M. Piasecki, P. Bragiel, M. G. Brik, Y. Gandhi and N. Veeraiah, Structural investigations on PbO–Sb_2O_3–B_2O_3:CoO glass ceramics by means of spectroscopic and dielectric studies, *J. Phys.: Condens. Matter*, vol. 21, pp. 245104, May 2009.

[40] A. M. Babeer, M.I. Sayyed, H. Y. Amin, Abd El-razek Mahmoud, M.S. Sadeq, Composition impacts of La_2O_3 on the structure and radiation shielding parameters of NiO–BaO–B_2O_3 glasses, *Opt. Mater.*, vol. 147, pp. 114622, January 2024.

[41] M. Purnima, S. Stalin, A. Edukondalu, M.A. Samee, S. Kareem Ahmmad, S. Rahman, Spectroscopic studies on Li_2O–MgO–Bi_2O_3–B_2O_3 glasses, *Chin. J. Phys.*, vol. 66, pp. 517-526, August 2020.

[42] M.E. Lines, A.E. Miller, K. Nassau, K.B. Lyons, Absolute raman intensities in glasses: II. Germania-based heavy metal oxides and global criteria, *J. Non-Cryst. Solids*, vol. 89, pp. 163-180, January 1987.

[43] A. McGlashan, Peter N. Nelson, P. Syam Prasad, M. Iezid, F. Goumeidane, R. Rajaramakrishna, P. Venkateswara Rao, Physical, thermal, optical, shielding and elastic properties of Bi_2O_3–B_2O_3–TeO_2 glass system doped with Fe_2O_3, *Radiat. Phys. and Chem.*, vol. 217, pp. 111444, April 2024.

[44] L. Tichy, H. Ticha, L. Herzigova, J. Ozdanova, Some physical properties of $(Bi_2O_3)x(BaO)0.5-x(B_2O_3)0.5$ glasses, *Mater. Chem. Phys.*, vol. 126, pp. 289-294, March 2011.

[45] F. He, Z. He, J. Xie, and J. Li, Y. IR and Raman Spectra Properties of Bi_2O_3-ZnO-B_2O_3-BaO Quaternary Glass System, *Am. J. Anal. Chem.*, vol. 5, pp. 1142-1150, November 2014.

[46] S. Thakur, V. Thakur, A. Kaur, L. Singh, Structural, Optical and thermal properties of nickel doped bismuth borate glasses, *J. Non-Cryst. Solids.*, vol. 512, pp. 60–71, July 2019.

[47] N. Gupta, A. Kaur, A. Khanna, F. Gonz` alez, C. Pesquera, R. Iordanova, B. Chen, Structure-property correlations in TiO_2 -Bi_2O_3-B_2O_3-TeO_2 glasses, *J. Non-Cryst. Solids*, vol. 470, pp. 168–177, September 2017.

[48] W. Gao, J. Wang, S. Cao, L. Li, J. Han, Bond characteristics, microstructure, and microwave dielectric properties of Bi_2O_3–ZnO–B_2O_3 glass-ceramics with Li_2O substitution, *Ceram. Int.*, vol. 50, pp. 5927-5935, February 2024.

[49] H. Ticha, J. Schwarz, L. Tichy, Raman spectra and optical band gap in some PbO-ZnO-TeO_2 glasses, *Mater. Chem. Phys.*, vol. 237, pp. 121834, November 2019.

[50] Y. Ban, Z. He, F.Qin, D. Zhou, Y. Cong, T. Wu, Y. Wu, Influence of La_2O_3 on the structural and luminescence properties in Er^{3+}/Ho^{3+} co-doped TeO_2-BaF_2-ZnF_2 glass, *Ceram. Int.*, Available online, January 2025.

[51] E.I. Kamitsos, G.D. Chryssikos, Borate glass structure by Raman and infrared spectroscopies, *J. Mol. Struct.*, vol. 247, pp. 1-16, July 1991,

[52] A. Madhu, N.S. Abd EL-Gawaad, S. Ali Osman Abdallah, Sunanda T. Dadami, B.G. Hegde, T. Uthayakumar, MB. Karthik Kumar, N. Srinatha, Unravelling the conductivity behaviour of thermally stable Li_2O– Bi_2O_3–B_2O_3–P_2O_5 glasses embedded with V_2O_5, *Ceram. Int.*, vol. 49, pp. 28781-28793, September 2023.

[53] O. Pravakar, T. Siddaiah, P.V.R.K. Ramacharyulu, N.O. Gopal, Ch. Ramu, H. Nagabhushana, Spectroscopic, thermal, structural and electrical studies on VO^{2+} ions doped PVA/MAA:EA polymer blend films, *J. Sci.: Adv. Mater. Dev.*, vol. 4, pp. 267-275, June 2019.

[54] B. Srinivas, A. Hameed, R. Vijaya Kumar, M. Narasimha Chary, and Md. Shareefuddin, Experimental and theoretical investigations on the EPR parameters and molecular orbital bonding coefficients of VO^{2+} ions in BTTB glasses. *Phil. Mag.*, vol. 98, pp. 1625–1640, March 2018.

[55] A. Davis, N.F. Mott, Conduction in non-crystalline systems V. Conductivity, optical absorption and photoconductivity in amorphous semiconductors, *Phil. Mag*., vol. 22, pp. 903–922, Jun 1970.

[56] J. Tauc, A. Menth, States in the gap, *J. Non-Cryst. Solids*., vol. 8, pp. 569–585, June 1972.

[57] A. S. Alqarni, N.N. Yusof, A. A. Kassimu, I. Bulus, I. M. Danmallam, S. Hashim, H. A. Thabit, Exploring the physio-elastic properties and optical band gap energies of boro-telluro-dolomite glasses infused with Nd_2O_3 dopants, *Optik*, vol. 288, pp. 171149, October 2023.

[58] A. El Boukili, L. Boudad, M. Taibi, M. El Amraoui, J. Aride, M. Rouzières, H. Saadaoui, Synthesis and investigation of the V_2O_5 effect on the properties of Na_2O–NiO-(1-x)P_2O_5–xV_2O_5 ($0 \leq x \leq 0.6$) system, *Ceram. Int.*, vol. 50, pp. 1693-1705, January 2024.

[59] J. S. Alzahrani, A. V. Lebedev, S. A. Avanesov, A. Hammoud, Z.A. Alrowaili, Z. M.M. Mahmoud, I.O. Olarinoye, C. Sriwunkum, M.S. Al-Buriahi, Synthesis, optical properties and radiation shielding performance of TeO_2-Na_2O-BaO-WO_3 glass system, *Optik*, vol. 261, pp. 169167, July 2022.

[60] A. Rani, R. Parmar, R.S. Kundu, Structural, physical and optical study of calcium modified bismuth borovanadate glasses: V_2O_5-B_2O_3-Bi_2O_3-CaO, *Opt. Mater*., vol. 143, pp. 114135, September 2023,

[61] T. Satyanarayana, K. Chandra Sekhar, K.M. Nissamudeen, Md. Shareefuddin, Unveiling the structural properties of $K_2B_4O_7$–$Li_2B_4O_7$–TeO_2–CuO glass: A comprehensive analysis using UV, EPR, FTIR and Raman spectroscopy, *Opt. Mater*., vol. 157, pp. 116425, November 2024.

[62] M. Montesso, D. Manzani, J. P. Donoso, C. J. Magon, I. D.A. Silva, M. Chiesa, E. Morra, M. Nalin, Synthesis and structural characterization of a new $SbPO_4$-GeO_2 glass system, *J. Non-Cryst. Solids*, vol. 500, pp. 133-140, November 2018.

[63] S. Bahammam, S. Abd El Al, F.M. Ezz-Eldin, Synthesis and characterization of γ-irradiated cadmium-borate glasses doped V_2O_5, *Results Phys*., vol. 7, pp. 241-249, 2017.

[64] A. Madhu, C.M. Joseph, Sunanda T. Dadami, N. Srinatha, Structural and spectroscopic studies of V_2O_5 incorporated lithium-bismuth-boro-tellurite glass ceramics, *Mater. Today: Proc*., vol. 62, pp. 5489-5493, 2022.

[65] D.L. Griscom, Electron spin resonance in glasses, *J. Non-Cryst. Solids*, vol. 40, pp. 211-272, July 1980.

[66] A. Abragam, B. Bleaney, Electron Paramagnetic Resonance of Transition Ions, *Oxford University* Press, 1970.

[67] M. Naga Sireesha, J. Suresh Krishna, V. Vinay Krishna, Ch. Linga Raju, Structural and spectroscopic properties of V_2O_5 doped zinc bismuth sodium borate glasses, *Mater. Today: Proc*., vol. 80, pp. 840-845, 2023.

[68] B. Srinivas, A. Hameed, G. Srinivas, M. Narasimha Chary, Md. Shareefuddin, Influence of V_2O_5 on physical and spectral (optical, EPR & FTIR) studies of SrO-TeO_2-TiO_2-B_2O_3 glasses*, Optik*, vol. 225, pp. 165815, January 2021.

[69] N. Rama Krishna Chand, B.K. Sudhakar, G. Ravikumar, V. Gayathri, P. Devika, T. Vennela, G. Srinivasa Rao, Ch.Srinivasa Rao, Influence of multi valent states of vanadium ions in ZnO doped novel calcium fluoro phosphate bio glasses, *J. Mech. Behav. Biomed. Mater.*, vol. 131, pp. 105230, July 2022.

[70] C.J. Ballhausen, H.B. Gray, The electronic structure of the vanadyl ion, *Inorg. Chem*., vol. 1, pp. 111–122, February 1962.

[71] B. Yasoda, R.P. Sreekanth Chakradhar, J.L. Rao, N.O. Gopal,EPR and optical absorption studies of VO^{2+} ions in alkaline earth aluminoborate glasses, *Mater. Chem. Phys*., vol. 106, pp. 33-38, November 2007.